Transport Analysis of Radial Electric Field in Helical Plasmas

S. Toda and K. Itoh

National Institute for Fusion Science, Oroshi-cho 322-6, Toki 509-5292, Japan

E-mail: toda.shinichiro@LHD.nifs.ac.jp

Abstract. A set of transport equations is analyzed which induces the radial transition of the electric field. A temperature profile which is related with the transport barrier is obtained by use of the theoretical model for the anomalous transport diffusivities. A dependence on the different initial condition is found even if the same values of the control parameters are used in calculations. A study of the temporal evolution of E_r is done. We examine the test of the adopted theoretical model for the anomalous transport diffusivities compared with the experimental result in Large Helical Device (LHD).

1. Introduction

The steep gradient in the radial electric field is obtained in the inner plasma region and the transport barrier was confirmed in the Electron Cyclotron Resonance Heating (ECRH) plasma in the compact helical system (CHS) [1] as well as in the Large Helical Device (LHD) [2]. A pulsating behavior of electrostatic potential (or the radial electric field) is also observed in the core region in CHS, illustrating a new dynamical state in magnetically-steady-state plasmas [3]. In Wendelstein7-AS (W7-AS), studies on the change of the electron transport triggered by the neoclassical transport were also done theoretically [4] and experimentally [5, 6]. More recently, a change in the anomalous transport in the core region was reported in W7-AS [7]. We have examined the one-dimensional transport equations which describe the temporal evolutions of the density, the electron and ion temperatures, and the radial electric field in a cylindrical configuration. The radial electric filed is assumed to be determined by the ambipolar condition for the neoclassical particle flux. The generation of the electric field in helical systems could be investigated more quantitatively because the neoclassical transport is found to play the dominant role in generating the radial electric field [8, 9]. We have used the transport model for anomalous diffusivities to describe the turbulent plasma. This model has been confirmed by the present observations in CHS experiments so long as the static profile is concerned [10].

In this article, the stationary structure of the radial electric field is examined and the hysteresis characteristic is found to form the shear layer of the radial electric field. Next,

we study the dynamics of the radial electric field in the core plasmas. Furthermore, the reduction of the heat diffusivity is qualitatively evaluated from the theoretical results. We compare the analytic results with the experimental results in LHD, and discuss the validity of the theoretical model for the anomalous transport diffusivities.

2. One-dimensional model transport equations

In this section, the model equations used here are shown. The cylindrical coordinate is used and r-axis is taken in the radial cylindrical plasma in this article. The region $0 \leq r \leq a$ is considered, where a is the minor radius. The expression for the radial neoclassical flux associated with helical-ripple trapped particle is given as [11]

$$\Gamma_j^{na} = -\epsilon_t^2 \sqrt{\epsilon_h} v_{dj}^2 n_j \int_0^\infty dx x^{\frac{5}{2}} e^{-x} \widetilde{\nu}_j \frac{A_j(x, E_r)}{\omega_j^2(x, E_r)}, \tag{1}$$

where $x \equiv m_j v^2/(2T_j)$, $A_j(x, E_r) = n_j'/n_j - Z_j e E_r/T_j + (x - 3/2)T_j'/T_j$, $\omega_j^2(x, E_r) = 3\widetilde{\nu}_j^2(x) + 1.67(\epsilon_t/\epsilon_h)(\omega_E + \omega_{Bj})^2 + (\epsilon_t/\epsilon_h)^{\frac{3}{2}}\omega_{Bj}^2/4 + 0.6\,|\omega_{Bj}|\,\widetilde{\nu}_j$ and $\widetilde{\nu}_j(x) = \nu_{thj}/(\epsilon_h x^{\frac{3}{2}})$. Here, the relations $\omega_E = -E_r/(rB)$, $\omega_{Bj} = -T_j \epsilon_h' x/(Z_j e r B)$ and $v_{dj} = -T_j/(Z_j e r B)$ are used for the species j. The parameters ϵ_t and ϵ_h are the toroidal and helical ripple, respectively. The prime denotes the derivative with respect to the radial direction. The total particle flux Γ^t is written as

$$\Gamma^t = \Gamma^{na} - D_a \frac{\partial n}{\partial r}. \tag{2}$$

Here, D_a is the anomalous particle diffusivity. The energy flux related with neoclassical ripple transport is given as [11]

$$Q_j^{na} = q_j^{na} + \frac{5}{2}\Gamma_j^{na} T_j = -\epsilon_t^2 \sqrt{\epsilon_h} v_{dj}^2 n_j T_j \int_0^\infty dx x^{\frac{7}{2}} e^{-x} \widetilde{\nu}_j(x) \frac{A_j(x, E_r)}{\omega_j^2(x, E_r)}. \tag{3}$$

The total heat flux Q_j^t of the species j is written as

$$Q_j^t = Q_j^{na} - n\chi_{aj} \frac{\partial T_j}{\partial r} - \frac{3}{2} D_a \frac{\partial n}{\partial r} T_j, \tag{4}$$

where χ_{aj} is the anomalous heat diffusivity for the species j. A theoretical model for the anomalous heat conductivity obtained by the eigenvalue problem for the ballooning mode and the interchange mode is adopted and will be explained later. The neoclassical diffusion coefficient for the electric field is expressed by [12]

$$D_{E_j} = -\frac{e}{\epsilon_\perp} \frac{3}{16\sqrt{2\pi}} \frac{Z_j e}{T_j} \frac{n_j \nu_{thj} T_j^4}{(Z_j e)^4} \frac{\epsilon_t^4}{\sqrt{\epsilon_h}} \left(1 + \frac{\epsilon_t}{\epsilon_h}\right) \int_{x_b}^\infty \frac{dx e^{-x} x^3}{\left(|E_r| + \left|x \frac{T_j}{Z_j e} \epsilon_h'\right|\right)^4}, \tag{5}$$

where $x_b = \left[\nu_{thj}/\left(\epsilon_h \left(|E_r| + |T_j/(Z_j e)\epsilon_h'|\right)\right)\right]^{2/3}$ and $\epsilon_\perp$ is the perpendicular dielectric coefficient as $\epsilon_\perp = \epsilon_0((c^2/v_A^2) + 1)(1 + 2q^2)$. The anomalous diffusion coefficient for the radial electric field is denoted by D_{Ea}.

The equation for the density is

$$\frac{\partial n}{\partial t} = -\frac{1}{r}\frac{\partial}{\partial r}(r\Gamma^t) + S_n, \tag{6}$$

where the term S_n represents the particle source. The equation for the electron temperature is given as

$$\frac{3}{2}\frac{\partial}{\partial t}(nT_e) = -\frac{1}{r}\frac{\partial}{\partial r}(rQ_e^t) - \frac{m_e}{m_i}\frac{n}{\tau_e}(T_e - T_i) + P_{he}, \tag{7}$$

where the term τ_e denotes the electron collision time and the second term in the right hand side represents the heat exchange between ions and electrons. The term P_{he} represents the absorbed power due to the ECRH heating and its profile is assumed to be proportional to $\exp(-(r/(0.2a))^2)$ for simplicity. The equation for the ion temperature is

$$\frac{3}{2}\frac{\partial}{\partial t}(nT_i) = -\frac{1}{r}\frac{\partial}{\partial r}(rQ_i^t) + \frac{m_e}{m_i}\frac{n}{\tau_e}(T_e - T_i) + P_{hi}. \tag{8}$$

The term P_{hi} represents the absorbed power of ions and its profile is also assumed to be proportional to $\exp(-(r/(0.2a))^2)$.

The radial electric field equation in a nonaxisymmetric system is expressed by [12, 13]

$$\frac{\partial E_r}{\partial t} = -\frac{e}{\epsilon_\perp}\sum_j Z_j\Gamma_j^{na} + \frac{1}{r}\frac{\partial}{\partial r}(\sum_j Z_j(D_{Ej} + D_{Ea})r\frac{\partial E_r}{\partial r}). \tag{9}$$

Equation (9) is solved together with the density and the temperature (ion and electron) equations (6), (7) and (8) as an initial value problem.

3. Boundary conditions and the model of anomalous transport coefficients

The density, temperature and electric field equations (6)-(9) are solved under the appropriate boundary conditions. We fix the boundary condition at the center of the plasma (r=0) such that $n' = T_e' = T_i' = E_r = 0$. For the diffusion equation of the radial electric field, the boundary condition at the edge ($r = a$) is chosen as $\sum_j Z_j\Gamma_j = 0$. This simplification is employed because the electric field bifurcation in the core plasma is the main subject of this study. The boundary conditions at the edge ($r = a$) with respect to the density are those expected in CHS device: $-n/n' = 0.05$m, $-T_e/T_e' = -T_i/T_i' = 0.02$m in this paper.

The machine parameters are similar to those of CHS device, such as $R = 1$m, $a = 0.2$m, the toroidal magnetic field $B = 1$T, toroidal mode number $m = 8$ and the poloidal mode number $\ell = 2$. We set the safety factor and the helical ripple coefficient as $q = 3.3 - 3.8(r/a)^2 + 1.5(r/a)^4$ and $\varepsilon_h = 0.231(r/a)^2 + 0.00231(r/a)^4$, respectively [1]. The particle source S_n is set to be $S_n = S_0\exp((r-a)/L_0)$, where L_0 is set to be 0.1m if the source is the ionization from the wall and the value of S_0 is strongly influenced by the particle confinement time.

In this article, we adopt the model for the anomalous heat diffusivity based on the theory of the self-sustained turbulence due to the ballooning mode and the interchange mode, both driven by the current difffusivity [14, 15] as a candidate. The reduction of the anomalous transport due to the inhomogeneous radial electric field was reported in

the toroidal helical system. The anomalous transport coefficient for the temperatures is given as $\chi_a = \chi_0/(1 + G\omega_{E1}^2)$, where $\chi_0 = F(s,\alpha)\alpha^{\frac{3}{2}}c^2 v_A/(\omega_{pe}^2 qR)$ and ω_{pe} is the electron plasma frequency. The factor $F(s,\alpha)$ is the function of the magnetic shear s and the normalized pressure gradient α, defined by $s = rq'/q$ and $\alpha = -q^2 R\beta'$. For the ballooning mode turbulence for the system with a magnetic well, we employ the anomalous thermal conductivity $\chi_{a,BM}$. The details about the coefficients $F(s,\alpha)$, G, and the factor ω_{E_1}, which stands for the effect of the electric field shear, are given in ref. [14] in the ballooning mode turbulence. In the case of the interchange mode turbulence for the system of the magnetic hill [15], we adopt the the anomalous thermal conductivity $\chi_{a,IM}$. The details about F, G, and the factor ω_{E_1} in the case of the interchange mode were given in ref. [15]. The greater one of these two diffusivities is adopted, $\chi_a = \max(\chi_{a,BM}, \chi_{a,IM})$. The different values for χ_a of electrons and ions are used here, *e.g.*, we set $\chi_{ae} = \chi_a$ for electrons and $\chi_{ai} = \chi_a/3$ for ions. Since we focus the case when the electron temperature is much higher than the ion temperature, the value of electrons of the anomalous transport diffusivity can be assumed to be larger than that of ions. The value for the anomalous diffusivities of the particle is set as $D_a = \chi_{ae}$ to include the effect of the radial and temporal variation of D_a in the results of analysis. The approximation $D_{Ea} = \chi_{ae}$ is employed throughout this paper, where the validity of this was discussed in ref. [16].

4. Results of transport analysis

4.1. Stationary solutions with transport barrier

When we calculate coupled equations (6)-(9), the absorbed power of electrons is 100kW and the coefficient S_0 is $7 \times 10^{22}\mathrm{m}^{-3}\mathrm{s}^{-1}$ for the choice of the anomalous transport coefficients in the previous section, where there is no absorbed power of ions. Using theses parameters and boundary conditions given, we analyze equations (6)-(9). The stationary solutions of the radial electric field are shown in figure 1(a) for the line-averaged density: $\bar{n} = 3.4 \times 10^{19}\mathrm{m}^{-3}$, the line-averaged electron temperature: $\bar{T}_e = 310\mathrm{eV}$ and the line-averaged ion temperature: $\bar{T}_i = 170\mathrm{eV}$ as the results of the calculation, where $\rho = r/a$. The density and the temperature profiles of the electrons and the ions are obtained in figures 1(b) and (c), respectively. In figure 1(c), the dashed curve represents the case of the ion temperature and the full curve shows the profile of the electron temperature, respectively. At the point ($\rho = \rho_T(0.38)$), the transition of the radial electric field is found. We can find multiple solutions of the electric field which satisfy the local ambipolar condition $\sum_j Z_j \Gamma_j^{na} = 0$ from the calculated profiles of the density and the temperatures of figure 1(b) and (c). The hard transition occurs when the a transition takes place between the multiple solutions for the local ambipolar condition. In the case of figure 1(a), the electron root for $\rho < \rho_T$ is sharply connected to the ion root for $\rho > \rho_T$ between them. The detailed confirmation of the transport calculation results with Maxwell's construction [17, 18] was done [19]. In this case (figure 1(a)), it

is confirmed that the radial transition of E_r satisfies Maxwell's construction.

It is found that there is a clear transport barrier in the electron temperature profile in figure 1(c). In figure 2(a), the anomalous transport diffusivities of electrons χ_{ae} is shown with the solid line. At the transition layer, the reduction of χ_{ae} is obtained due to the strong gradient of the electric field. The value of the anomalous transport diffusivities of ions χ_{ai} is a third of χ_{ae}. The neoclassical diffusivities of electrons χ_e^{NEO} and ions χ_i^{NEO} are also shown with the dashed line and the dotted line, respectively. In the case of the spatial transition in figure 1(a), the electric field goes across zero at $\rho \approx \rho_T$. Therefore, the neoclassical diffusivities have a peak near the surface where the relation $E_r \approx 0$, because they depend on the value of E_r itself. This is specially obvious in the case of ions. In figure 2(b), the sum of the anomalous and the neoclassical diffusivities is shown. The case of electrons and the case of ions are obtained with dashed line and the dotted line, respectively. The total suppression of electron transport can be clearly seen, because the explicit reduction of the anomalous transport of electrons are obtained.

4.2. Dependence on initial conditions and hysteresis effect

We study the dependence on initial conditions of the obtained steady calculation results in this subsection. At first, we obtain two stationary solutions for different external parameters and use them as two different initial conditions. They have the positive E_r (electron root) and the negative E_r (ion root) in the entire radial region, respectively. The former can be obtained for the parameter $S_0 = 5 \times 10^{22}\mathrm{m}^{-3}\mathrm{s}^{-1}$ and the latter can be obtained for for the parameter $S_0 = 1 \times 10^{23}\mathrm{m}^{-3}\mathrm{s}^{-1}$, respectively. The other input parameters, such as the absorbed power of electrons and ions, are same as the previous subsection. In the former case, the line-averaged density $\bar{n} = 1.6 \times 10^{19}\mathrm{m}^{-3}$, the line-averaged electron temperature $\bar{T}_e = 0.54\mathrm{keV}$ and the line-averaged ion temperature $\bar{T}_i = 0.11\mathrm{keV}$ are obtained. In the latter case, $\bar{n} = 4.5 \times 10^{19}\mathrm{m}^{-3}$, $\bar{T}_e = 0.23\mathrm{keV}$ and $\bar{T}_i = 0.16\mathrm{keV}$.

Next, we analyze the coupled equations (6)-(9) using these steady states as two initial conditions. We use the parameter in terms of the particle source as $S_0 = 7 \times 10^{22}\mathrm{m}^{-3}\mathrm{s}^{-1}$. The absorbed power of electrons is 100kW and the absorbed power of ions is 10kW, respectively. That is, in the first case, S_0 increases from $5 \times 10^{22}\mathrm{m}^{-3}\mathrm{s}^{-1}$ to $7 \times 10^{22}\mathrm{m}^{-3}\mathrm{s}^{-1}$ at $t = 0$. In the second case, S_0 is reduced from $10^{23}\mathrm{m}^{-3}\mathrm{s}^{-1}$ to $7 \times 10^{22}\mathrm{m}^{-3}\mathrm{s}^{-1}$ at $t = 0$. In both cases, S_0 is kept constant at the same value for $t > 0$ and the state reaches the steady one. A difference between two kinds of the calculations is only the initial conditions. Figure 3 shows the radial profiles of the steady states, E_r in figure 3(a), n in figure 3(b), T_e in figure 3(c) and T_i in figure 3(d). The solid line represents the results starting from the states of the electron root at an initial condition. The dotted curve shows the obtained steady state evolving from the states of the ion root at an initial condition. In the case that the steady state is obtained from the initial condition of the electron root, the positive E_r in the core ($\rho < 0.5$) region is retained

and the solution in the outer region becomes negative. In the case as shown with the solid line in figure 3(a), the transition of the radial electric field occurs at the transition layer and the region of the positive E_r is found to be sharply connected to that of the negative E_r between them. In contrast, if the steady state is obtained from the initial condition of ion root in the entire radial region, the radial electric field E_r takes the negative value in the entire radial region as is shown by the dotted line in figure 3(a). This difference only comes from two different kinds of the initial conditions. In the case when the positive value of E_r is shown in the core region, the change of the gradient for T_e and T_i can be seen with the solid lines in figure 3(c) and (d), respectively. Therefore, the formation of the transport barrier depends on the history of the control parameters. Furthermore, the influence of the history of the control parameters on the achieved stationary solutions appears dominantly in the core ($\rho < 0.5$), not in the outer region ($\rho > 0.5$).

Temporal oscillation of E_r was already obtained in the plasma edge region [20, 21]. In the present work, the dependence on different kinds of initial conditions is shown specially in the core region. That is, a hysteresis effect is shown to exist in the core electric field. However, the state of the temporal oscillation of E_r is not yet obtained in the core region.

5. Test of a theoretical model for the anomalous transport diffusivities

We adopt a theoretical model for the anomalous transport diffusivities driven by the current diffusivity as a candidate in the previous section. In this section, we discuss the validity of this model comparing the calculation results with the experimental results in LHD. When we analyze equations (6)-(9) in this section, we set the machine parameters which are similar to those of LHD; $R = 3.6$m, $a = 0.6$m, $B = 3$T, $m = 10$, $\ell = 2$. We use the typical profile in LHD as $q = 1/\left(0.4 + 1.2\rho^2\right)$ and $\varepsilon_h = 2\sqrt{1-(2/(mq(0)-1)^2)}I_2(mr/R)$, respectively. Here, $q(0)$ is the value of the safety factor at $r = 0$ and I_2 is the second order modified Bessel function. The boundary conditions and the profiles of particle source and heating used in this section are same as those shown in the previous section. The theoretical model for the anomalous transport is also same as those in the previous section. The absorbed power of electrons and ions is 1MW and 0W, respectively and set constant in time. The profiles of the particle source and the heating source are also same as those in the previous section. To simulate the experimental procedure of decreasing density, the value of the parameter S_0 with respect to the particle source linearly decreases from $10^{25}\mathrm{m}^{-3}\mathrm{s}^{-1}$ to $10^{23}\mathrm{m}^{-3}\mathrm{s}^{-1}$ during the time 0.1s. In this parameter region examined here, the typical energy confinement time is about 0.01s. The characteristic time of the temporal change of the density is around 0.01s. To examine the reduction of the heat transport, the total electron diffusivity $\chi_{etotal}(=\chi_{ae}+\chi_e^{NEO})$ normalized by the gyro-Bohm factor $T_e^{3/2}$ is plotted in figure 4 at $\rho = 0.2$ as the function of R/L_{T_e}, where $L_{T_e} = -T_e/T_e'$. The total electron diffusivity χ_{etotal} normalized by $T_e^{3/2}$ is considered to be constant when the transport

barrier is not formed. When the radial profile of E_r takes ion root in the all radial region and the electron root is not seen at an initial time, the normalized $\hat{\chi}$ at $\rho = 0.2$ takes the value $25\mathrm{m}^2\mathrm{s}^{-1}\mathrm{keV}^{-3/2}$, namely L-mode state, where $\hat{\chi} \equiv \chi_{etotal}/T_e^{3/2}$. After the density decreases and the jump to the electron root in the E_r profile is obtained in the core region, the value of $\hat{\chi}$ at $\rho = 0.2$ decreases to $8\mathrm{m}^2\mathrm{s}^{-1}\mathrm{keV}^{-3/2}$ in figure 4. Therefore, the improvement factor from the L-mode state to the improved state with the transport barrier takes the value 3.2. We can also examine the dependence of $\hat{\chi}$ on R/L_{T_e} such as $\hat{\chi} \propto (R/L_{T_e})^{-2.2}$ in the improved state shown with dotted line in figure 4. From the experimental results in LHD [2], this improvement factor can be estimated as the value 20 and the dependence of $\hat{\chi}$ on R/L_{T_e} is shown as $\hat{\chi} \propto (R/L_{T_e})^{-5.2}$ in the improved state. Comparing the indexes of the power law derived from the calculation result and the experimental result, the dependence of $\hat{\chi}$ on R/L_{T_e} in both cases are found to be qualitatively so similar that the calculation by use of this theoretical model can reproduce the dependence of the normalized heat diffusivity of electrons on the temperature gradient. There are quantitative differences between the indexes of the power law and the improvement factors derived from the calculation result and the experimental result. These differences may come from the different situations of the calculation and the experiment. For example, the absorbed power of electrons decreases when the state becomes to the improved one (the electron root) in the experimental result. The absorbed power of electrons is kept temporally constant even in the improved state in the present theoretical work.

6. Conclusions

In this paper, the structure of the radial electric field in helical plasmas is theoretically studied. The spatial and temporal evolutions of the plasma density, the temperatures and the radial electric field are examined. The analysis is done by use of one-dimensional transport model equations. Theoretical model of the ballooning mode or the interchange mode is adopted for the anomalous transport diffusivities. At first, the steady state of the radial electric field is shown and a hard transition between the multiple ambipolar E_r, which induces a steep gradient of E_r, is obtained. The clear transport barrier and the transport reduction are demonstrated. Next, the sensitivity to the initial conditions was found. Therefore, the initial condition can determine the final plasma state and crucial physical quantities such as the confinement time. The temporal oscillation of E_r can not be yet found in the core region although the sensitivity of the physical state to the initial condition is obtained. Simple test is done by comparing the calculation results and the experimental results to discuss the validity of the theoretical model used here. The dependence of the transport on the temperature gradient derived from the calculation result is found to qualitatively agree with that from the experimental results (LHD). However, there is a quantitative difference between them. In a future work, we will simulate much closer procedure to the experimental one.

Acknowledgments

The authors would like to acknowledge Prof. S. -I. Itoh, Prof. A. Fukuyama and Dr. M. Yagi for illuminating discussions. Discussions with Dr. A. Fujisawa, Prof. K. Ida and Prof. H. Sanuki are also appreciated. This work is partly supported by the Japanese Ministry of Education, Culture, Sports, Science and Technology, Grants-in-Aid for Scientific Research, Nos 14780393 and 15360495.

[1] Fujisawa A *et al* 2000 *Phys. Plasmas* **7** 4152
[2] Ida K *et al* 2003 *Phys. Rev. Lett.* **91** 085003
[3] Fujisawa A *et al* 1998 *Phys. Rev. Lett.* **81** 2256
[4] Maaßberg H *et al* 1993 *Plasma Phys. Control. Fusion* **35** B319
[5] Kick M, Maaßberg H, Anton M, Baldzuhn J, Endler M, Görner C, Hirsh M, Weller A, Zoletnik S and the W7-AS team 1999 *Plasma Phys. Control. Fusion* **41** A549
[6] Maaßberg H, Beidler C D, Gasparino U, Romé, the W7-AS team, Dyabilin K S, Marushchenko N B and Murakami S 2000 *Phys. Plasmas* **7** 295
[7] Stroth U, Itoh K, Itoh S -I, Hartfuss H, Laqua H, the ECRH team and the W7-AS team 2001 *Phys. Rev. Lett.* **86** 5910
[8] Kovriznykh L M 1984 *Nucl. Fusion* **24** 851
[9] Ida K 1998 *Plasma Phys. Control. Fusion* **40** 1429
[10] Toda S and Itoh K 2002 *Plasma Phys. Control. Fusion* **44** 325
[11] Shaing K C 1984 *Phys. Fluids* **27** 1567
[12] Hastings D E 1985 *Phys. Fluids* **28** 334
[13] Hastings D E, Houlberg W A, Shaing K C, 1985 Nucl. Fusion **25** 445
[14] Itoh K, Itoh S -I, Fukuyama A, Yagi M and Azumi M 1994 *Plasma Phys. Control. Fusion* **36** 279
[15] Itoh K, Itoh S -I, Fukuyama A, Sanuki H and Yagi M 1994 *Plasma Phys. Control. Fusion* **34** 123
[16] Itoh K, Itoh S -I, Fukuyama A, Yagi M and Azumi M 1993 *J. Phys. Soc. Jpn.* **62** 4269
[17] Schlögl F 1972 *Z.Physik* **253** 147
[18] Haken H 1976 Synergetics (Berlin:Springer) section 9.3
[19] Toda S and Itoh K 2004 *Plasma Phys. Control. Fusion* **46** 1039
[20] Hastings D E 1986 *Phys. Fluids* **29** 536
[21] Toda S and Itoh K 2003 *Division of Plasma Physics Meeting, APS, October 27-31, Albuquerque, NM* LP1.084

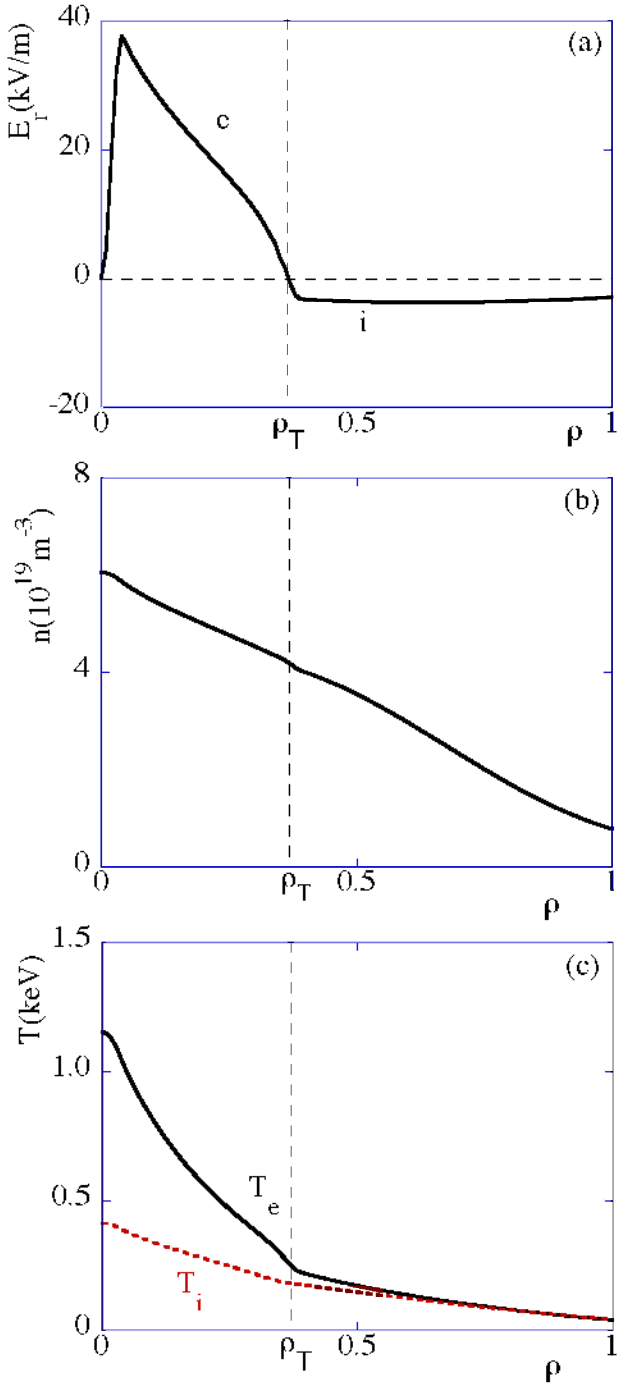

Figure 1. (a) Radial dependence of the electric field (full curve). (b) radial profile of the density. (c) profiles of the temperatures of ions and electrons. The absorbed power of electrons is 100kW and that of ions is 0kW, respectively. The coefficient S_0 of the particle source is $5 \times 10^{22}\mathrm{m}^{-3}\mathrm{s}^{-1}$.

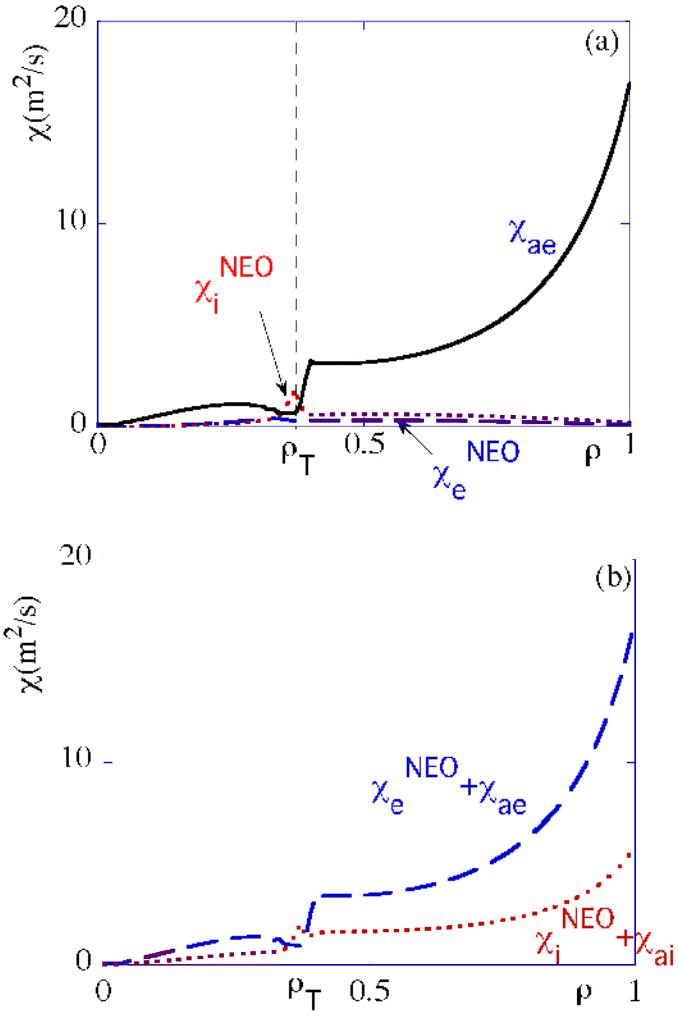

Figure 2. Radial profiles of the anomalous and neoclassical diffusivities in figure 2(a). In figure 2(b), the sum of the anomalous and neoclassical diffusivities is shown. These figures correspond to the case of figure 1.

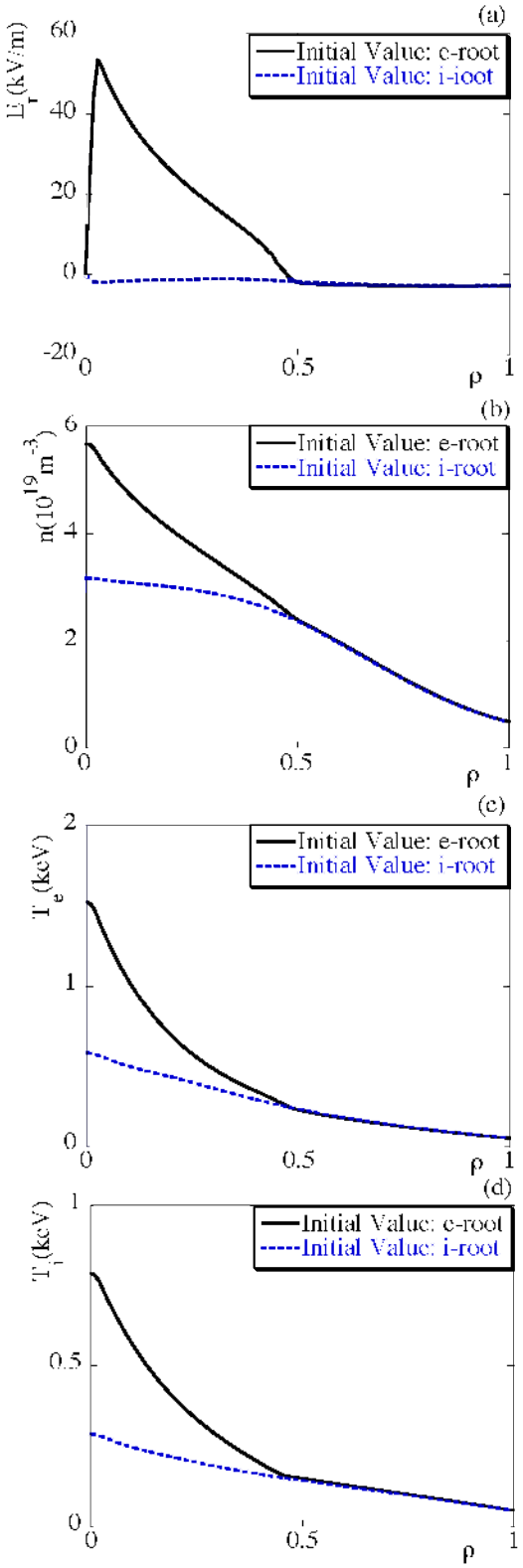

Figure 3. (a) Radial dependence of the electric field. (b) Radial profile of the density. (c) profiles of the electron temperature and (d) profiles of the ion temperature. The full curve and dotted curve show the steady state from the initial condition of the electron root and ion root. respectively. The absorbed power of electrons is 100kW and that of ions is 10kW, respectively. The coefficient S_0 of the particle source is $7 \times 10^{22}\mathrm{m}^{-3}\mathrm{s}^{-1}$.

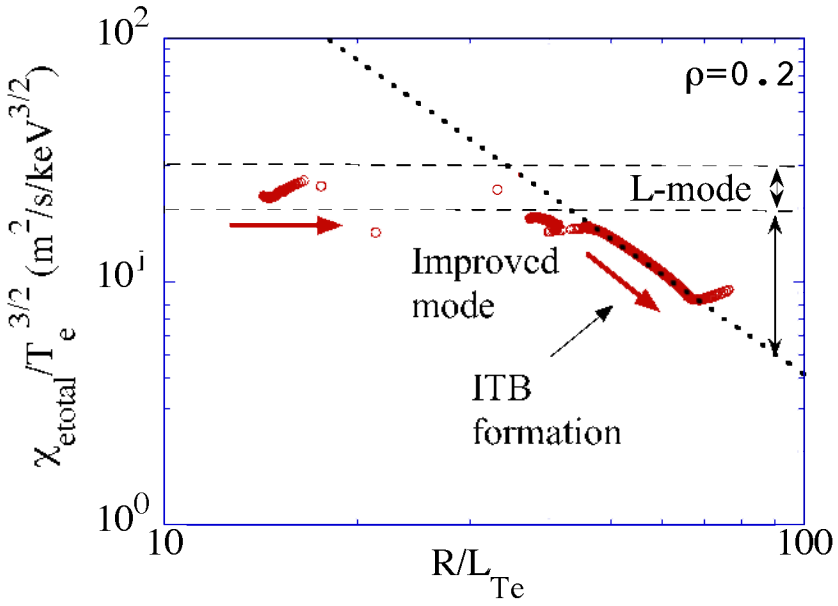

Figure 4. Normalized heat diffusivity calculated as a function of R/L_{T_e} at $\rho = 0.2$. The arrow indicates the temporal direction. The dotted line represents the relation $\chi_{etotal}/T_e^{3/2} \propto (R/L_{T_e})^{-2.2}$.